

# Analysis of Laser ARPES from $\text{Bi}_2\text{Sr}_2\text{CaCu}_2\text{O}_{8+\delta}$ in superconductive state: angle resolved self-energy and fluctuation spectrum

Jae Hyun Yun and Jin Mo Bok

*Department of Physics and Institute for Basic Science Research,  
SungKyunKwan University, Suwon 440-746, Korea.*

Han-Yong Choi

*Department of Physics and Institute for Basic Science Research,  
SungKyunKwan University, Suwon 440-746, Korea.  
School of Physics, Korea Institute for Advanced Study, Seoul 130-722, Korea.  
Asia Pacific Center for Theoretical Physics, Pohang 790-784, Korea.*

Wentao Zhang and X. J. Zhou

*National Laboratory for Superconductivity, Beijing National Laboratory for Condensed Matter Physics,  
Institute of Physics, Chinese Academy of Sciences, Beijing 100190, China.*

Chandra M. Varma

*Department of Physics and Astronomy, University of California, Riverside, California 92521.*

We analyze the ultra high resolution laser angle resolved photo-emission spectroscopy (ARPES) intensity from the slightly underdoped  $\text{Bi}_2\text{Sr}_2\text{CaCu}_2\text{O}_{8+\delta}$  in the superconductive (SC) state. The momentum distribution curves (MDC) were fitted at each energy  $\omega$  employing the SC Green's function along several cuts perpendicular to the Fermi surface with the tilt angle  $\theta$  with respect to the nodal cut. The clear observation of particle-hole mixing was utilized such that the complex self-energy as a function of  $\omega$  is directly obtained from the fitting. The obtained angle resolved self-energy is then used to deduce the Eliashberg function  $\alpha^2 F^{(+)}(\theta, \omega)$  in the diagonal channel by inverting the  $d$ -wave Eliashberg equation using the maximum entropy method. Besides a broad featureless spectrum up to the cutoff energy  $\omega_c$ , the deduced  $\alpha^2 F$  exhibits two peaks around 0.05 eV and 0.015 eV. The former and the broad feature are already present in the normal state, while the latter emerges only below  $T_c$ . Both peaks become enhanced as  $T$  is lowered or the angle  $\theta$  moves away from the nodal direction. The implication of these findings are discussed.

PACS numbers:

## I. INTRODUCTION

The recent observation of the particle-hole mixing in the superconductive (SC) state of the cuprates by high resolution angle-resolved photo-emission spectroscopy (ARPES) has opened up a new window to probe the fundamental physics of high temperature superconductivity.<sup>1,2</sup> In particular, an analysis of the spectra in the SC state, using the Eliashberg formalism for  $d$ -wave superconductivity, provides the fluctuation spectrum responsible for pairing. This is an extension of the tunneling experiments and analysis with which it was definitively established that the pairing in metals like Pb is through exchange of phonons.<sup>3</sup> It should be remembered that to get reliable information, it was necessary to have measurements of conductance at different temperatures and range of voltages of the order of the cut-off energy in the phonon spectrum to an accuracy of 0.2 %. The particle-hole mixing in cuprate superconductors was first observed some 15 years ago in ARPES.<sup>4</sup> Those experiments had much worse momentum and energy resolutions. Since the cut-off is an order of magnitude higher for the cuprates than Pb and the angle-dependence of the spectra is crucial, the demands on the quality of the data

are only being recently met through ultra-high resolution and stability of laser based ARPES.

The ARPES provided an early evidence for the  $d_{x^2-y^2}$  pairing state of the cuprates.<sup>5</sup> The measured leading edge shift of the energy distribution curve (EDC) of ARPES as a function of the tilt angle showed that the superconducting gap is consistent with the  $d$ -wave pairing gap. It ushered in more debates and experiments which eventually led to the establishment of the  $d$ -wave pairing symmetry for the cuprate superconductors.<sup>6</sup> The ARPES contains more information than the leading edge shift which may be utilized, for example, to extract the Eliashberg functions and track their evolution as the temperature is lowered below  $T_c$ . By properly extending the normal state analysis of extracting the self-energy, one should be able to deduce information about superconductivity of the cuprates such as the angle-resolved diagonal and off-diagonal self-energies, and the pertinent Eliashberg functions. This is precisely what we wish to present in this paper.

For this, we fitted the ARPES momentum distribution curves (MDC) at each energy  $\omega$  employing the SC Green's function along several cuts perpendicular to the Fermi surface with the tilt angle  $\theta$  from the nodal cut

with respect to the  $(\pi, \pi)$  in the Brillouin zone. The clear observation of particle-hole mixing was utilized such that the complex self-energy as a function of  $\omega$  is directly obtained from fitting the ARPES data. Thus obtained angle resolved diagonal self-energy  $\Sigma(\theta, \omega)$  is then used to deduce the Eliashberg function  $\alpha^2 F^{(+)}(\theta, \omega)$ , i.e., the bosonic fluctuation spectrum multiplied by the coupling constant squared, in the diagonal channel by inverting the  $d$ -wave Eliashberg equation using the maximum entropy method (MEM). The diagonal self-energy evolves smoothly into the normal state self-energy as the temperature is raised above  $T_c$ . The evolution of the Eliashberg function as the temperature or tilt angle is varied will reveal a useful information about the nature of superconductivity in the cuprates.

On the other hand, the angle resolved off-diagonal self-energy  $\phi(\theta, \omega)$ , or, the density of states  $N(\theta, \omega)$  given by Eq. (6) below, can be used for  $d$ -wave superconductors to extract the Eliashberg function in the off-diagonal (i.e., pairing) channel<sup>7</sup> as the ordinary tunneling conductance was used by McMillan and Rowell to extract the spectrum of fluctuations for  $s$ -wave superconductors.<sup>3</sup> While the Eliashberg functions along the diagonal and off-diagonal channels are assumed to be the same for the  $s$ -wave pairing, they are in general different for  $d$ -wave superconductors. The current approach has the unique advantage in that it can disentangle the Eliashberg functions in the diagonal and off-diagonal channels,  $\alpha^2 F^{(+)}(\theta, \omega)$  and  $\alpha^2 F^{(-)}(\theta, \omega)$ , respectively.

In the following section II, we will present the formulation of the MDC analysis of the ARPES intensity in the superconducting state using the full momentum and energy dependence of SC Green's function. It is an extension of the ARPES analysis in the normal state.<sup>8</sup> The results for the diagonal self-energy  $\Sigma(\theta, \omega)$  from slightly underdoped Bi2212 will be presented in section III at temperatures above and below  $T_c$  and along several cuts of the tilt angle  $\theta$  with respect to the  $(0, 0) - (\pi, \pi)$  nodal cut. As in the normal state, the extracted self-energy may be used as an input to deduce the Eliashberg function  $\alpha^2 F^{(+)}(\theta, \omega)$ . The obtained Eliashberg functions are presented in section IV. Recall that  $\alpha^2 F^{(+)}(\theta, \omega)$  along different cuts collapse onto a single curve with a peak near 0.05 eV below the angle dependent cutoff  $\omega_c(\theta)$  in the normal state.<sup>8</sup> In the SC state the peak around 0.05 eV gets enhanced and additional peak emerges around 0.015 eV below  $T_c$ . Both peaks become enhanced as  $T$  is lowered or the tilt angle is increased. We will conclude the paper by making some remarks and outlooks in the section V.

## II. FORMALISM

The ARPES intensity, within the sudden approximation, is given by

$$I(\mathbf{k}, \omega) = |M(\mathbf{k}, \nu)|^2 f(\omega) [A(\mathbf{k}, \omega) + B(\mathbf{k}, \omega)], \quad (1)$$

where  $M(\mathbf{k}, \nu)$  is the matrix element,  $\nu$  the energy of incident photon,  $f(\omega)$  the Fermi distribution function,  $A(\mathbf{k}, \omega)$  the quasiparticle (qp) spectral function, and  $B(\mathbf{k}, \omega)$  is the background from the scattering of the photo-electrons. We write the in-plane momentum  $\mathbf{k}$  with the distance from the  $(\pi, \pi)$  point  $k_\perp$  and the tilt angle measured from the nodal cut  $\theta$  as shown in Fig. 1. The self-energy has a much weaker dependence on  $k_\perp$  than  $\theta$  or  $\omega$  as will be discussed below. Assuming this, the spectral function is written as

$$A(\mathbf{k}, \omega) = -\frac{1}{\pi} \text{Im} G(\mathbf{k}, \omega),$$

$$G(\mathbf{k}, \omega) = \frac{W(\theta, \omega) + Y(\mathbf{k}, \omega)}{W^2(\theta, \omega) - Y^2(\mathbf{k}, \omega) - \phi^2(\theta, \omega)}, \quad (2)$$

where  $G(\mathbf{k}, \omega)$  is the retarded Green's function in the superconductive state. The following notations were used:

$$\begin{aligned} W(\theta, \omega) &= \omega Z(\theta, \omega) = \omega - \Sigma(\theta, \omega), \\ Y(\mathbf{k}, \omega) &= \xi(\mathbf{k}) + X(\theta, \omega), \\ \phi(\theta, \omega) &= Z(\theta, \omega) \Delta(\theta, \omega), \end{aligned} \quad (3)$$

where  $Z(\theta, \omega)$  is the renormalization function,  $X(\theta, \omega)$  the shift of the qp dispersion, and  $\Sigma(\theta, \omega)$  and  $\phi(\theta, \omega)$  represent the qp diagonal self-energy and the off-diagonal self-energy, respectively. The equation that connects  $\Sigma(\theta, \omega)$ ,  $X(\theta, \omega)$ , and  $\phi(\theta, \omega)$  with the effective interaction in the charge and spin channels is the Eliashberg equation.<sup>9</sup> It is presented in section IV below in connection with extraction of the Eliashberg functions.

It is informative to make the following decomposition of the SC Green's function:

$$\frac{Y + W}{Y^2 - (W^2 - \phi^2)} = \frac{1/2 + N/2}{Y - P} + \frac{1/2 - N/2}{Y + P}, \quad (4)$$

where

$$P(\theta, \omega) = \sqrt{W^2(\theta, \omega) - \phi^2(\theta, \omega)}, \quad (5)$$

$$N(\theta, \omega) = \frac{W(\theta, \omega)}{\sqrt{W^2(\theta, \omega) - \phi^2(\theta, \omega)}}. \quad (6)$$

We note that the qp dispersion shift  $X(\theta, \omega)$  vanishes in the particle-hole symmetric band. Although the symmetry does not hold for the realistic tight-binding dispersion, it holds to a good degree over the small energy scale of SC and the renormalization is neglected in the present work. The ARPES intensity divided by the Fermi distribution function is then given by

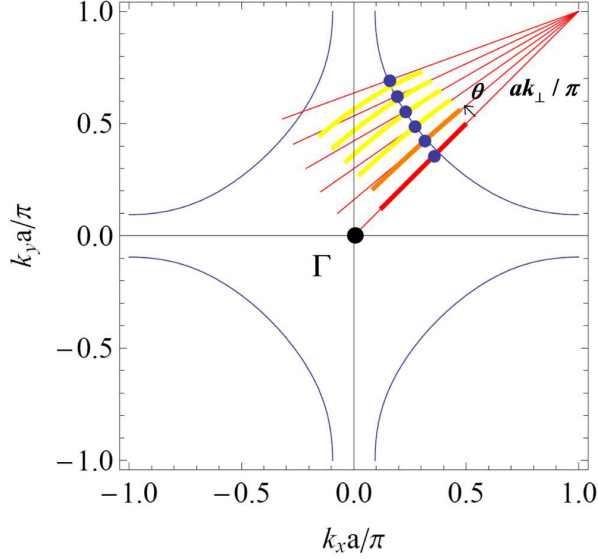


FIG. 1: The Fermi surface of Bi2212 in the Brillouin zone. The blue solid curves centered around the  $\Gamma$  point is the FS from Eq. (48) and the solid dots are the experimentally determined FS at  $\theta = 0^\circ, 5^\circ, 10^\circ, 15^\circ, 20^\circ, 25^\circ$ .  $k_\perp$  is the distance from the  $(\pi, \pi)$  point. The yellow thick curves along each cut indicate the actual momentum paths at  $\omega = 0$  of the experimentally measured ARPES MDC data.

$$\frac{I(\theta, k_\perp, \omega)}{f(\omega)} = C(\theta, \omega) \text{Im} \left[ \frac{1 + N(\theta, \omega)}{\xi(\mathbf{k}) - P(\theta, \omega)} + \frac{1 - N(\theta, \omega)}{\xi(\mathbf{k}) + P(\theta, \omega)} \right] + B(\theta, \omega), \quad (7)$$

where  $C(\theta, \omega)$  is the weight of the spectral function of the ARPES intensity. We then have the six parameter fit in SC state:  $C$ ,  $B$ , the real and imaginary parts of  $P$  and  $N$  as a function of binding energy  $\omega$ , while the normal state fitting required four parameters. Note that the dependence on  $k_\perp$  comes in through the bare dispersion  $\xi(\mathbf{k})$  only. It is therefore important to take appropriate dispersion.

As in the normal state, we used the tight-binding (TB) dispersion and the linear dispersion (LD) for the MDC analysis. The TB dispersion  $\xi(\mathbf{k})$  is given by

$$\xi(k_x, k_y) = -2t(\cos k_x a + \cos k_y a) + 4t' \cos k_x a \cos k_y a - 2t''(\cos 2k_x a + \cos 2k_y a) - \mu, \quad (8)$$

where  $a = 3.82 \text{ \AA}$  is the lattice constant and  $\mu$  is the chemical potential. We took  $t = 0.395$ ,  $t' = 0.084$ ,  $t'' = 0.042$ , and  $\mu = -0.43 \text{ eV}$ . The linear dispersion was determined by linearization of the TB at FS of the six tilt angles  $\theta$ .

$$\xi(\theta, k_\perp) = v_F(\theta) [k_\perp - k_F(\theta)], \quad (9)$$

where  $v_F(\theta)$  and  $k_F(\theta)$  are Fermi velocity and Fermi momentum, respectively. The experimentally determined

FS in comparison with that from Eq. (8) is shown in Fig. 1. The six cuts with the tilt angles  $\theta$  with respect to the  $(\pi, \pi)$  are also shown with the solid lines.

Note that the first and the second terms in Eq. (7) give the intensity due to the “particle” and the “hole” parts of the Bogoliubov particles, respectively.  $P(\theta, \omega)$  and  $N(\theta, \omega)$  are directly extracted from fitting the ARPES MDC data. Then,

$$\Sigma(\theta, \omega) = \omega - P(\theta, \omega)N(\theta, \omega), \quad (10)$$

$$\phi^2(\theta, \omega) = P^2(\theta, \omega)[N^2(\theta, \omega) - 1] \quad (11)$$

gives  $\Sigma(\theta, \omega)$  and  $\phi(\theta, \omega)$ . Since the density of states  $N(\theta, \omega) = 1$  in the normal state, the off-diagonal self-energy  $\phi(\theta, \omega)$  can only be extracted from the difference of the spectra between the normal and SC state. These differences are very small at energies above a few times  $T_c$ . So the requirements on the ARPES data to reliably extract  $\phi$  at higher energies are considerably more stringent than those to extract  $\Sigma$ . We defer this to future work and show here that considerable information on the fluctuation spectrum can be extracted from the diagonal self-energy alone.

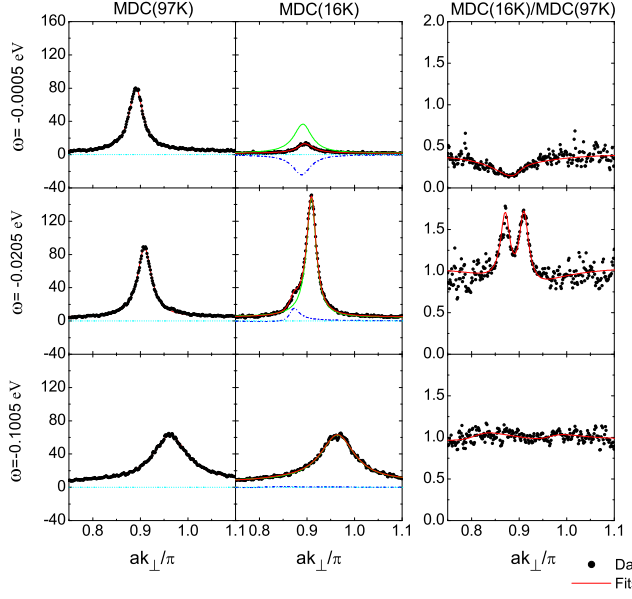


FIG. 2: The representative MDC as a function of the momentum along the tilt angle  $\theta = 20^\circ$ . The dots are the experimental data and the solid red lines are the fitting. The first and second columns show the fittings in the normal state and in the SC state, respectively. The last column is the MDC ratios of SC to normal states.

### III. THE MDC ANALYSIS

The ultra high resolution Laser ARPES data were collected from slightly underdoped Bi2212 of SC critical temperature  $T_c = 89$  K and pseudogap temperature  $T^* \approx 160$  K. The data were taken along the cuts of the tilt angle  $\theta = 0$  (nodal cut), 5, 10, 15, 20, and 25 degrees with respect to the nodal direction and at temperatures  $T = 107, 97$  above  $T_c$  and 80, 70, and 16 K below  $T_c$ . The photon energy of  $h\nu = 6.994$  eV was used in the laser ARPES. Refer to Ref.<sup>8</sup> for more detailed description of the experimental setup and the technical details.

Typical results of the ARPES analysis in SC state are given in Fig. 2 for the tilt angle  $\theta = 20^\circ$ . The first column shows the results in the normal state at  $T = 97$  K as a function of the magnitude of the inplane momentum  $k_\perp$  from the  $(\pi, \pi)$  point at the energy  $\omega = -0.0005$ ,  $-0.0205$ , and  $-0.1005$  eV. The three energies represent the cases of  $\omega \ll \Delta$ ,  $\omega \approx \Delta$ , and  $\omega \gg \Delta$ , where  $\Delta$  is the gap amplitude at  $\theta = 20^\circ$  and  $T = 16$  K,

$$\Delta = \frac{\phi(\theta, \Delta)}{Z(\theta, \Delta)}. \quad (12)$$

The symbols are the data and the red solid lines are the fitting results. The agreements are almost perfect which justifies the neglect of the  $k_\perp$  dependence of the self-

energy. The second column is the corresponding results deep in the SC state at  $T = 16$  K. The green solid (blue dashed) lines are the particle (hole) branch of the fitting, the first (second) term of Eq. (7).

The important point is that the hole branch represented by the blue curves exhibits a peak as a consequence of the particle-hole mixing of the pairing. This can be most spectacularly seen near  $\omega \approx \Delta$  presented in the middle row. In addition to the main peak near  $k_\perp a/\pi \approx 0.91$  from the original qp branch, there exists the secondary peak at  $k_\perp a/\pi \approx 0.87$ . This is a direct observation of the particle-hole mixing deep in the SC state. The details of observations are presented separately.<sup>1</sup> The particle-hole mixing was previously reported in the EDC by observing the bending-back of the spectral peaks.<sup>4</sup> Both branches of the Bogoliubov dispersion due to the particle-hole mixing were also reported by the EDC in the intermediate temperature regime<sup>2</sup> because in the low temperature limit the Fermi function cuts the hole branch off and close to  $T_c$  the pairing feature is very weak. The mixing is observed in the low temperature regime here and will be utilized to obtain information about superconductivity in the cuprates. The last row shows the case of  $\omega \gg \Delta$ . As the energy increases above  $\Delta$ , the hole branch contribution vanishes as the bottom plots show. The last column is the ratios of the MDC at 16 K to 97 K which show the hole branch more clearly.

We now show the real part of the extracted self-energy along the tilt angle  $\theta = 0$  and  $\theta = 20^\circ$  in Fig. 3(a) and (b), respectively, and that at  $T = 16$  K in the plot (c). Fig. 3(a) and 3(b) demonstrate that the feature around 0.05–0.07 eV is already present in the normal state and is enhanced as the temperature is lowered, while the broad feature continues from the normal to SC state with no discernible change within the accuracy of the experiment. The 0–0.02 eV feature emerges only along off-nodal cuts below  $T_c$  as can be seen from the plots (a) and (b), and its energy scale increases as the tilt angle is increased as can be seen from the plot (c). This is consistent with the  $d$ -wave pairing gap and implies that the 0–0.02 eV feature is induced by superconductivity.

### IV. THE ELIASHBERG FUNCTION

The extracted diagonal and off-diagonal self-energies may be used as experimental inputs to deduce the Eliashberg functions  $\alpha^2 F^{(+)}(\theta, \omega)$  and  $\alpha^2 F^{(-)}(\theta, \omega)$  by inverting the Eliashberg equation. The  $d$ -wave Eliashberg equation may be written as

$$\Sigma(\theta, \omega) = \int_{-\infty}^{\infty} d\epsilon \int_{-\infty}^{\infty} d\epsilon' S(\omega, \epsilon, \epsilon') N_1(\epsilon) \alpha^2 F^{(+)}(\theta, \epsilon') \quad (13)$$

$$\phi(\omega) = - \int_{-\infty}^{\infty} d\epsilon \int_{-\infty}^{\infty} d\epsilon' S(\omega, \epsilon, \epsilon') D_1(\epsilon) \alpha^2 F^{(-)}(\epsilon') \quad (14)$$

$$S(\omega, \epsilon, \epsilon') = \frac{f(\epsilon) + n(-\epsilon')}{\epsilon + \epsilon' - \omega - i\delta} \quad (15)$$

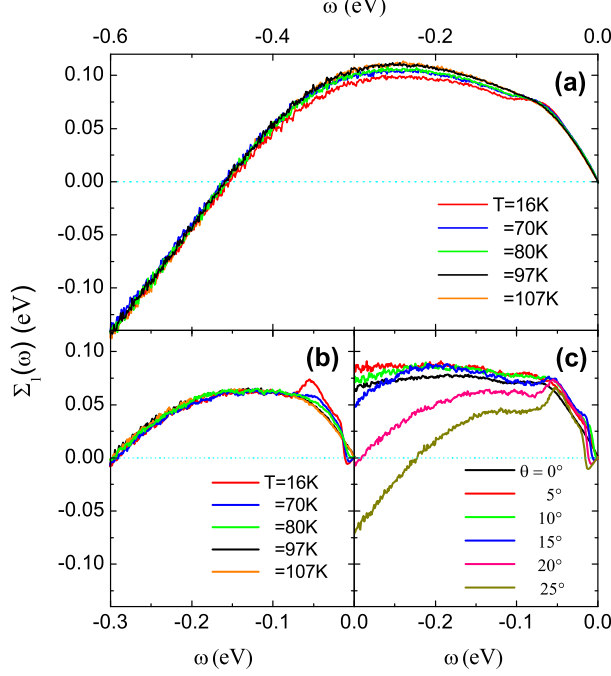


FIG. 3: The real part of the extracted self-energy. The plots (a) and (b) are along the nodal cut and  $\theta = 20^\circ$ , respectively, and the plot (c) is at temperature  $T = 16$  K.

where  $f$  and  $n$  represent the Fermi and Bose distribution functions, respectively.

We took

$$\phi(\theta, \omega) = \phi(\omega) \sin(2\theta) \quad (16)$$

because the pairing is  $d$ -wave, and use the notations

$$N_1(\epsilon) \equiv \left\langle \text{Re} \frac{W(\theta', \epsilon)}{\sqrt{W^2(\theta', \epsilon) - \phi^2(\epsilon) \sin^2(2\theta')}} \right\rangle_{\theta'} \quad (17)$$

$$D_1(\epsilon) \equiv \left\langle \frac{1}{v_F(\theta')} \text{Re} \frac{\phi(\epsilon) \sin^2(2\theta')}{\sqrt{W^2(\theta', \epsilon) - \phi^2(\epsilon) \sin^2(2\theta')}} \right\rangle_{\theta'} \quad (18)$$

$$\alpha^2 F^{(+)}(\theta, \epsilon') \equiv \left\langle \frac{\alpha^2(\theta, \theta')}{v_F(\theta')} F^{(+)}(\theta, \theta', \epsilon') \right\rangle_{\theta'} \quad (19)$$

where  $v_F(\theta')$  is the angle-dependent Fermi velocity and the bracket implies the angular average over  $\theta'$ .

As in the normal state, we invert the real part of the Eliashberg equation to deduce the Eliashberg function  $\alpha^2 F^{(+)}(\theta, \epsilon')$  using the real part of the extracted diagonal self-energy as an input. As mentioned before, the requirement on the data and numerical fitting are considerably stringent to reliably extract the off-diagonal self-energy than to extract the diagonal self-energy. We will defer the deduction of  $\alpha^2 F^{(-)}(\theta, \omega)$  to future work and

focus on  $\alpha^2 F^{(+)}(\theta, \omega)$  here. The real part of Eq. (13) may be written as

$$\Sigma_1(\theta, \omega) = \int_{-\infty}^{\infty} d\omega' K(\omega, \omega') \alpha^2 F^{(+)}(\theta, \omega'),$$

$$K(\omega, \omega') = \int_{-\infty}^{\infty} d\epsilon \mathcal{P} \frac{f(\epsilon) + n(-\omega')}{\epsilon + \omega' - \omega} N_1(\epsilon) \quad (20)$$

where  $\mathcal{P}$  represents the principal value, and the subscripts 1 and 2 refer to the real and imaginary parts. The inversion was performed using the maximum entropy method.<sup>8,10</sup> Recall that in the normal state the Eliashberg functions along different cuts of the tilt angle  $\theta$  all collapse onto a single curve which has a small peak at  $\approx 0.05$  eV, flattens above 0.1 eV, and vanishes above the angle dependent cutoff  $\omega_c(\theta)$ .  $\omega_c(\theta) \approx 0.35 - 0.4$  eV along the nodal direction and decreases as  $\theta$  increases.<sup>8</sup>

Fig. 4, showing the deduced  $\alpha^2 F^{(+)}(\theta, \omega)$ , is the key results of the present paper. The deduced function is noisier at larger angles. The noise somewhat depends on the multiplier  $\alpha$  of the maximum entropy method.<sup>19</sup> We believe most of the oscillatory behavior seen are artifacts of the MEM analysis and will focus only on the robust features whose variation is continuous as a function of temperature and angles. The broad feature above about 0.07 eV does not change with angle or with temperature. It is a continuation of that required for the marginal Fermi liquid properties which were derived recently to arise from quantum criticality.<sup>11</sup> It carries about 3/4 of the total spectral weight.

The plot 4(a) is slightly below  $T_c$  at  $T = 80$  K. The Eliashberg function does not change much from the normal state shape except that the peak value at  $\omega \approx 0.05$  eV increases to approximately 0.4 for large tilt angles from 0.3 of the normal state value. In Fig. 4(b),  $\alpha^2 F^{(+)}(\theta, \omega)$  along the nodal cut is shown as the temperature is varied. As might be expected from above behavior, there is little change along the nodal cut, although there is a sign of the lower energy peak at  $T = 16$  K. It seems that the change in  $\Sigma(\theta = 0, \omega)$  as  $T$  is varied as shown in Fig. 3(a) is predominantly from the change in the density of states that enters Eq. (20).

$\alpha^2 F^{(+)}(\theta, \omega)$  deep in the SC state is shown in Fig. 4(c). Like at  $T = 80$  K, the peak at  $\omega = 0.05$  has its normal state value for small tilt angle and increases as the angle increases. Also a second peak at  $\approx 0.015$  eV emerges which, like the  $\omega \approx 0.05$  eV peak, increases from the normal state value as the angle is increased. In Fig. 4(d), the Eliashberg function along the cut  $\theta = 20^\circ$  is shown. As the temperature is lowered below  $T_c$ , the 0.05 eV peak is enhanced and the 0.015 eV peak newly develops, as one can anticipate from preceding discussion. Both peaks are enhanced as  $T$  is lowered or the tilt angle is increased.

There have been many investigations of the fluctuation spectrum of the cuprate superconductors such as the infrared conductivity, inelastic neutron scattering, Raman scattering, scanning tunneling spectroscopy, and so on, which are less direct in the information they provide for

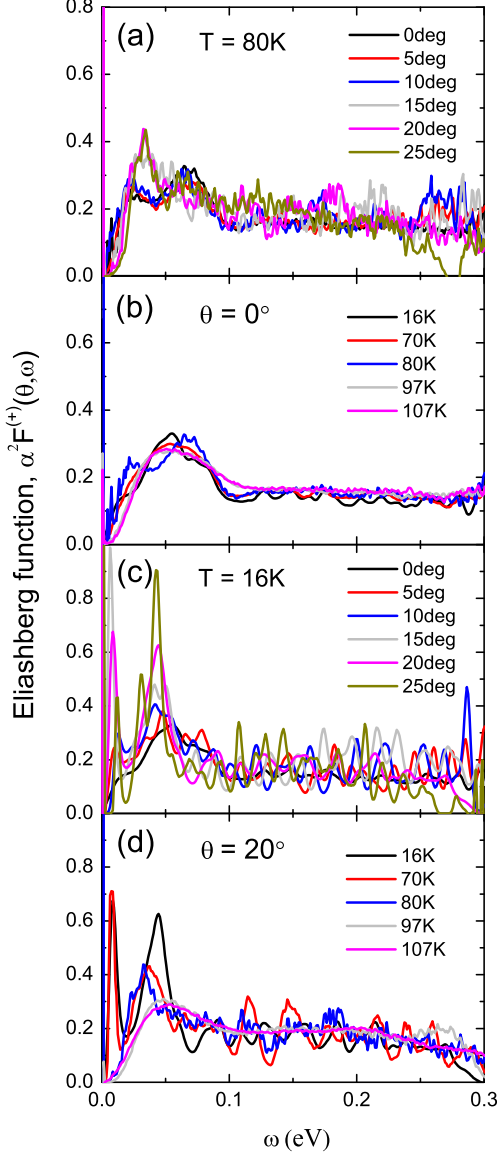


FIG. 4: The deduced Eliashberg function  $\alpha^2 F^{(+)}(\theta, \omega)$ . Plot (a) is at  $T = 80$  K slightly below  $T_c$ , plot (b) along the nodal cut, plot (c) at  $T = 16$  K deep in the SC state, and (d) is along the off-nodal cut of  $\theta = 20^\circ$ .

the source of superconductivity than ARPES. Analysis of the frequency dependent conductivity by the McMaster group reported that a single peak shows up in the Eliashberg function below 0.1 eV for  $\text{Bi}_2\text{Sr}_2\text{CaCu}_2\text{O}_{8+\delta}$  and other cuprate compounds, but a double peak feature for  $\text{La}_{1.83}\text{Sr}_{0.17}\text{CuO}_4$  at low temperatures. It exhibits a peak at  $\omega \approx 0.05$  eV at high temperature  $T = 250$  K, but as  $T$  is lowered to 30 K it showed two peaks at 0.015 and 0.044 eV.<sup>12</sup> The inelastic neutron scattering (INS) experiment on  $\text{La}_{1.84}\text{Sr}_{0.16}\text{CuO}_4$  also reported the two peak structure around 0.018 and 0.04 – 0.07 eV at the

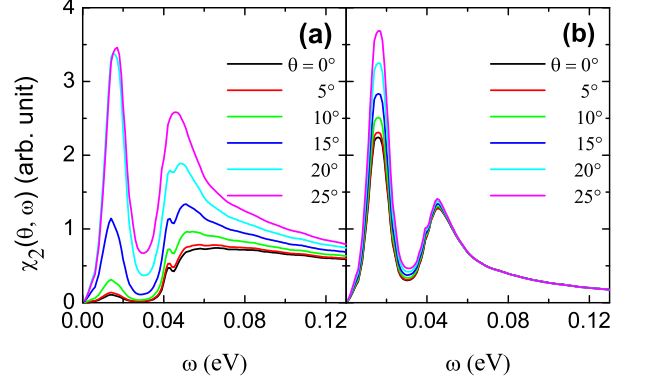


FIG. 5: The  $\theta'$  averaged susceptibility  $\chi_2(\theta, \omega)$  calculated from Vignolle to compare with  $\alpha^2 F^{(+)}(\theta, \omega)$ . The plot (a) is the  $\chi_2(\theta, \omega)$  from Vignolle and (b) is with the correlation length reduced to 0.1 of (a).

antiferromagnetic wave vector.<sup>13</sup> The Eliashberg analysis of the break junction SIS conductance and scanning tunneling spectra on overdoped  $\text{Bi}_2\text{Sr}_2\text{CaCu}_2\text{O}_{8+\delta}$  reported a single peak near  $\approx 0.02$  eV.<sup>14</sup>

No inelastic neutron scattering results are available for  $\text{Bi}_2\text{Sr}_2\text{CaCu}_2\text{O}_{8+\delta}$ , so that we can only compare our results with the detailed extraction of the spectral function of the magnetic fluctuations  $\chi(\mathbf{k}, \omega)$  for  $\text{La}_{1.84}\text{Sr}_{0.16}\text{CuO}_4$ . The positions of the two peaks around 0.018 and 0.04 – 0.07 eV are consistent with the peak positions of the deduced  $\alpha^2 F^{(+)}(\theta, \omega)$ . To make comparison of the momentum dependence between our  $\alpha^2 F^{(+)}(\theta, \omega)$  and INS results of  $\chi_2(\mathbf{q}, \omega)$ , we compute  $\chi_2(\theta, \omega)$  by taking the integral over  $\theta'$  with both  $\mathbf{k}$  and  $\mathbf{k}'$  on the Fermi surface having the tilt angles  $\theta$  and  $\theta'$ , respectively. As with Eq. (19), we take

$$\chi_2(\theta, \omega) \equiv \langle \chi_2(\mathbf{k} - \mathbf{k}', \omega) \rangle_{\theta'} . \quad (21)$$

The imaginary part of the spin susceptibility  $\chi_2(\mathbf{q}, \omega)$  was taken from Vignolle *et al.* INS results.<sup>13</sup> Fig. 5(a) is the computed  $\chi_2(\theta, \omega)$  from Vignolle and (b) is that with the correlation length reduced to 1/10 of (a). Comparing with our results in Fig. 4, the variation with angle compares better with the reduced correlation length. The angle independence of the flat part of  $\alpha^2 F^{(+)}(\theta, \omega)$  is consistent only with the fluctuation spectrum which has the short correlation length on the scale of the lattice constant.

The origin of the  $\sim 50$  meV feature is often taken to be a phonon<sup>15,16</sup> but it may be the strong dispersionless magnetic feature recently observed<sup>17,18</sup> only in the pseudogap region in the cuprates. One may be able to decide between the two through ARPES analysis similar to that done here of overdoped samples without the pseudogap.

## V. CONCLUDING REMARKS

We have presented the analysis of the ARPES intensity in the superconductive state for the Eliashberg function along the diagonal channel,  $\alpha^2 F^{(+)}(\theta, \omega)$ . Beside the broad featureless spectrum, a peak at 0.05 eV present in the normal state is enhanced as  $T$  is lowered, and a second peak emerges around 0.015 eV in the SC state. The 0.015 eV peak is an interesting new feature which needs further exploration. Since it appears only below  $T_c$ , it can not be responsible for  $T_c$ . We do not have an answer at present to the question as to what kind of collective modes of the superconducting state it represents.

The origin of the 50 meV feature generally observed is at the heart of current debate. One may be able to answer through ARPES analysis similar to that done here of overdoped samples without the pseudogap.

## Acknowledgments

This work was supported by National Research Foundation (NRF) of Korea through Grant No. NRF 2010-0010772. CMV's work is partially supported by NSF grant DMR-0906530.

- 
- <sup>1</sup> W. Zhang, J. M. Bok, J. H. Yun, G. Liu, L. Zhao, H. Liu, J. Meng, X. Dong, J. Zhang, W. Lu, et al., submitted to Phys. Rev. Lett. (2011).
  - <sup>2</sup> H. Matsui, T. Sato, T. Takahashi, S.-C. Wang, H.-B. Yang, H. Ding, T. Fujii, T. Watanabe, and A. Matsuda, Phys. Rev. Lett. **90**, 217002 (2003).
  - <sup>3</sup> W. L. McMillan and J. M. Rowell, Phys. Rev. Lett. **14**, 108 (1965).
  - <sup>4</sup> J. C. Campuzano, H. Ding, M. R. Norman, M. Randeria, A. F. Bellman, T. Yokoya, T. Takahashi, H. Katayama-Yoshida, T. Mochiku, and K. Kadowaki, Phys. Rev. B **53**, R14737 (1996).
  - <sup>5</sup> Z.-X. Shen, D. S. Dessau, B. O. Wells, D. M. King, W. E. Spicer, A. J. Arko, D. Marshall, L. W. Lombardo, A. Kapitulnik, P. Dickinson, et al., Phys. Rev. Lett. **70**, 1553 (1993).
  - <sup>6</sup> D. A. Wollman, D. J. Van Harlingen, W. C. Lee, D. M. Ginsberg, and A. J. Leggett, Phys. Rev. Lett. **71**, 2134 (1993).
  - <sup>7</sup> I. Vekhter and C. M. Varma, Phys. Rev. Lett. **90**, 237003 (2003).
  - <sup>8</sup> J. M. Bok, J. H. Yun, H.-Y. Choi, W. Zhang, X. J. Zhou, and C. M. Varma, Phys. Rev. B **81**, 174516 (2010).
  - <sup>9</sup> A. W. Sandvik, D. J. Scalapino, and N. E. Bickers, Phys. Rev. B **69**, 094523 (2004).
  - <sup>10</sup> W. H. Press, S. A. Teukolsky, W. T. Vetterling, and B. P. Flannery, *Numerical recipes* (Cambridge University Press, New York, 2002).
  - <sup>11</sup> V. Aji, A. Shekhter, and C. M. Varma, Phys. Rev. B **81**, 064515 (2010).
  - <sup>12</sup> J. Hwang, E. Schachinger, J. P. Carbotte, F. Gao, D. B. Tanner, and T. Timusk, Phys. Rev. Lett. **100**, 137005 (2008).
  - <sup>13</sup> B. Vignolle, S. M. Hayden, D. F. McMorro, H. M. Ronnow, B. Lake, C. D. Frost, and T. G. Perring, Nature Phys. **3**, 163 (2007).
  - <sup>14</sup> J. F. Zasadzinski, L. Ozyuzer, L. Coffey, K. E. Gray, D. G. Hinks, and C. Kendziora, Phys. Rev. Lett. **96**, 017004 (2006).
  - <sup>15</sup> A. Lanzara, P. Bogdanov, X. Zhou, S. Kellar, D. Feng, E. Lu, T. Yoshida, H. Eisaki, A. Fujimori, K. Kishio, et al., Nature **412**, 510 (2001).
  - <sup>16</sup> X. Zhou, T. Yoshida, A. Lanzara, P. Bogdanov, S. Kellar, K. Shen, W. Yang, F. Ronning, T. Sasagawa, T. Kakeshita, et al., Nature **423**, 398 (2003).
  - <sup>17</sup> Y. Li, V. Baledent, G. Yu, N. Barisic, K. Hradil, R. A. Mole, Y. Sidis, P. Steffens, X. Zhao, P. Bourges, et al., Nature **468**, 283 (2010).
  - <sup>18</sup> Y. He and C. M. Varma, Phys. Rev. Lett. **106**, 147001 (2011).
  - <sup>19</sup> The multiplier  $\alpha$  is a determinative parameter that controls how close the fitting should follow the data while not violating the physical constraints. When  $\alpha$  is small, the fitting will follow the data as closely as possible at the expense of a noisy and/or negative Eliashberg function, and when  $\alpha$  is large, the extracted Eliashberg function will not deviate much from the constraint function.